arXiv:1702.07455v1 [cond-mat.str-el] 24 Feb 2017

Quantum spin ice under a [111] magnetic field: from pyrochlore to kagomé

Troels Arnfred Bojesen[1] & Shigeki Onoda[1,2]

[1]*Quantum Matter Theory Research Team, RIKEN Center for Emergent Matter Science (CEMS), Wako, Saitama 351-0198, Japan, and*
[2]*Condensed Matter Theory Laboratory, RIKEN, Wako, Saitama 351-0198, Japan.*

Quantum spin ice [1,2], modeled for magnetic rare-earth pyrochlores, has attracted great interest for hosting a U(1) quantum spin liquid, which involves spin-ice monopoles as gapped deconfined spinons as well as gapless excitations analogous to photons [3,4]. However, the fate of these monopoles and photons under a [111] magnetic field remains open. In the classical case, a weak field aligns the spins on triangular-lattice layers, producing kagomé spin ice with a 2/3 magnetization plateau [5–7]. An increase in the field induces a direct discontinuous transition to a fully polarized state [8] through a perfect ionization and crystallization of monopoles [9]. In this Letter, we uncover for the quantum case that a supersolid [10–12] of monopoles, showing both a superfluidity and a partial ionization, intervenes kagomé spin ice and the fully polarized ionic monopole insulator. We also show that kagomé spin ice evolves towards a kagomé valence bond solid [13] on cooling.

There exists a prototype of magnetic rare-earth pyrochlores [14] that involve a strong geometrical frustration of interactions among effective pseudospin-1/2 moments located at the vertices of a corner-sharing network of tetrahedra (Fig. 1**a**). For instance, most of the low-temperature magnetic and thermodynamic properties in $Dy_2Ti_2O_7$ and $Ho_2Ti_2O_7$ (refs [4,8,15,16]) are practically described by the nearest-neighbor antiferromagnetic Ising model,

$$H_{\rm cl} = J \sum_{\langle \mathbf{r},\mathbf{r}' \rangle} S^z_{\mathbf{r}} S^z_{\mathbf{r}'}, \quad J > 0, \tag{1}$$

where $\mathbf{S}_{\mathbf{r}} = (S^x_{\mathbf{r}}, S^y_{\mathbf{r}}, S^z_{\mathbf{r}})$ represents a pseudospin-$\frac{1}{2}$ operator at a pyrochlore lattice site $\mathbf{r}$ in a C_2-invariant set of local spin frames [17,18] $(\mathbf{e}^x_\mu, \mathbf{e}^y_\mu, \mathbf{e}^z_\mu)$ with the sublattice index $\mu = 0, \cdots, 3$ (Fig. 1**b**). This interaction forces a 2-in, 2-out spin ice rule [15]: in each tetrahedron, the energy is minimized by two spins pointing inwards to and the other two outwards from the center (Fig. 1**d**), in an analogy to proton displacements in hexagonal water ice [19]. This leaves a residual ice entropy associated with the macroscopic degeneracy of the spin-ice-rule vacuums. Creating 3-in, 1-out or 1-in, 3-out local defects – monopoles – with which we assign a charge $Q = +1$ or -1 (Fig. 1**e**), costs half the spin-ice-rule interaction energy, $J/2$. These monopoles behave as static quasiparticles obeying an analogous Coulomb law and can only be excited thermally [4,8]. The average low-temperature pseudospin and monopole charge configuration, as well as its excitation spectrum, is depicted in Fig. 2**c**.

On the other hand, $Yb_2Ti_2O_7$ (refs [18,20]), $Tb_2Ti_2O_7$ (ref. [21]) and $Pr_2Zr_2O_7$ (ref. [22]) have been

understood as quantum spin ice [17,23] where spin-flip exchange interactions, for instance,

$$H_\perp = J_\perp \sum_{\langle \mathbf{r},\mathbf{r}'\rangle} \left(S^x_{\mathbf{r}} S^x_{\mathbf{r}'} + S^y_{\mathbf{r}} S^y_{\mathbf{r}'} \right), \tag{2}$$

become active in the background of the spin-ice-rule interaction $H_{\rm cl}$. Spin flips are accompanied by a transfer of monopole charge (Fig. 1**f**), so that the monopoles exhibit quantum kinematics as bosonic spinons, leading to a broadening of charge-1 exciations (Fig. 2**d**). If the spin-ice rule interaction dominates over the kinetic energy, the monopoles remain incompressible with an energy gap in their excitations. Then, a "diamagnetic current" and the associated "flux" generated by successive spin flips around closed paths (Fig. 1**g**) may be fixed. This deconfines the monopoles and leaves gapless spin excitations described by "photons" in a magnetic analogue of quantum electrodynamics [3,4] (Fig. 2**d** with $B = 0$). The quantum spin ice is now in what is called a U(1) quantum spin liquid state [3], as has been evidenced by quantum Monte-Carlo simulations on the minimal model $H_{\rm XXZ} = H_{\rm cl} + H_\perp$ for $0 > J_\perp > J_\perp^{\rm sf} = -0.104J$ (refs. [24,25]). Conversely, if the kinetic energy dominates over the spin-ice-rule interaction, as is the case when $J_\perp < J_\perp^{\rm sf}$, the monopoles are Bose-Einstein condensed and thus confined [26], resulting in a monopole superfluid (Fig. 2**e**). Note that the superfluid density of monopoles is proportional to a transverse spin stiffness ρ (see Methods). Hence, a finite monopole superfluid density points to a long-range order of transverse pseudospin components.

Now, of our interest are the fates of the monopoles and "photons" against a [111] magnetic field $\mathbf{B} = B\mathbf{e}_0$. The Hamiltonian reads

$$H = H_{\rm XXZ} - \mathbf{B} \cdot \sum_{\mathbf{R}_+} \mathbf{m}_{\mathbf{R}_+}, \quad \mathbf{m}_{\mathbf{R}_+} = \sum_{\mu=0}^{3} \mathbf{e}^z_\mu S^z_{\mathbf{R}_+ + \mathbf{b}_\mu} \tag{3}$$

with the magnetization $\mathbf{m}_{\mathbf{R}_+}$ of the "upward" oriented tetrahedron centered at $\mathbf{R}_+$ and the sublattice vector $\mathbf{b}_\mu$ measured from $\mathbf{R}_+$. We have assumed that only $S^z_{\mathbf{r}}$ couples to the magnetic field, as is the case for non-Kramers ions Pr^{3+} and Tb^{3+} (refs. [2,23]), e.g. in $Pr_2Ir_2O_7$ (ref. [27]), $Pr_2Zr_2O_7$ (refs. [22]), $Pr_2Hf_2O_7$ (ref. [28]), and $Tb_2Ti_2O_7$ (refs. [21,29]), where $S^x_{\mathbf{r}}$ and $S^y_{\mathbf{r}}$ correspond to electric quadrupoles [2,21,23]. In the classical limit, $J_\perp = 0$, B produces two successive transitions at zero temperature $T = 0$. (See the $J_\perp = 0$ plane of Fig. 2**b**.) First, an infinitesimally small B forces spins in the (111) triangular-lattice layers (Fig. 1**a**) to point in the field direction, i.e, $\langle S^z_{\mathbf{R}_+ + \mathbf{b}_0} \rangle = 1/2$, while the remaining spins in the (111) kagomé-lattice layer take a 2-in, 1-out configuration in each upward tetrahedron, leading to $\sum_{\mu=1}^{3} \langle S^z_{\mathbf{R}_+ + \mathbf{b}_\mu} \rangle = -1/2$ (Fig. 2**f**) and a magnetization plateau at $m = |\langle \mathbf{m}_{\mathbf{R}_+} \rangle| = 2/3$. The extensive degeneracy of spin ice partially remains within each kagomé layer, and hence the state is called kagomé spin ice [5–7]. At $B = 3J$, there occurs an abrupt spin-flip transition from 2-in, 2-out to the 3-in, 1-out fully polarized state with $m = 1$. Accordingly, the ionized monopole charge $\delta Q \equiv \langle Q_{\mathbf{R}_+} \rangle$ jumps from 0 to 1 (Fig. 2**g**), leading to an ionic monopole insulator. This transition has been dubbed a monopole crystallization [9]. Now systematic theoretical understandings in the quantum case are called for.

We perform quantum Monte-Carlo simulations (see Methods) on the minimal quantum spin

ice model given by Eq. (3) with $J_\perp < 0$. Figure 3 presents results on m, δQ and two components of the spin stiffness, $\rho_{(111)}$ and $\rho_{[111]}$, being normal and parallel to the field, for the particular case of $J_\perp = -0.15J < J_\perp^{\rm sf}$, in which the zero-field ground state is a monopole superfluid. Increasing B up to $\sim 0.1J$ at the lowest temperature, m arises from 0 with a finite slope, i.e., a finite [111] magnetic susceptibility. Both $\rho_{(111)}$ and $\rho_{[111]}$ steeply decay to zero, pointing that the monopole superfluid dies out quickly. Further increasing B up to $B_1 \sim 0.4J$, m increases to 2/3 without any apparent singularity. In these low-field ranges, monopoles are prevented from living on a long-time scale by the spin-ice-rule interaction, so $\delta Q = 0$. Similar behaviours of continuously increasing m, $\delta Q = 0$, and $\rho_{(111)} = \rho_{[111]} = 0$ appear from $B = 0$ when $J_\perp = -0.09J > J_\perp^{\rm sf}$ It suggests that the phase out of the monopole superfluid around $B = 0$ is adiabatically connected to the case with $J_\perp > J_\perp^{\rm sf}$ at $B = 0$, and hence it is a neutral monopole insulator, namely, a U(1) quantum spin liquid. From B_1 to $B_2 \sim 1.4J$, m is pinned to the 2/3 plateau where the spin-ice-rule constraint remains to be satisified on a long-time scale, i.e. $\delta Q = 0$, as in kagomé spin ice. In these field ranges, a nonzero δQ appears only with moderately large thermal excitations at around $T \sim 0.2$-$0.3J$ where a Schottky peak appears in the specific heat for $B = 0$ [25]. With further increasing B above B_2, m restarts increasing from 2/3 and simultaneously, δQ, $\rho_{(111)}$ and $\rho_{[111]}$ start increasing from zero. This establishes a monopole supersolid showing a partial ionization $0 < \delta Q < 1$ of monopoles and a long-range transverse spin order (Fig. 2**h**). The spin stiffness is strongly anisotropic with $\rho_{(111)}$ being an order of magnitude larger than $\rho_{[111]}$, indicating that the transverse spin order is triggered by correlations within kagomé layers. A further increase in B drives a phase transition to the inonic monopole insulator with $\rho_{(111)} = \rho_{[111]} = 0$. Reflecting that the monopole supersolid emerges because of a kinetic energy gain of monopoles, this phase shrinks with decreasing $|J_\perp|$ and is absent in classical spin ice systems. The lowest-temperature results are schematically summarized in Fig. 2**a**, and the global phase digram in Fig. 2**b**.

To understand the low-temperature properties in the kagomé spin ice plateau regime, we compute the spatial profiles of energy-integrated diffuse neutron-scattering cross-sections. Figure 4**a** shows the profile in the classical kagomé spin ice regime at $T = J/20$ and $B = 1.3J$. There appear short-range correlations associated with a broad peak at $\frac{2\pi}{a}(\frac{2}{3}, -\frac{2}{3}, 0)$ and symmetry-related points, in addition to a broadened pinch-point singularity at $\mathbf{q} = \frac{2\pi}{a}(\frac{2}{3}, \frac{2}{3}, -\frac{4}{3})$ and symmetry-related points, with a being the cubic lattice constant. The pattern clearly matches the experimental observation in $Dy_2Ti_2O_7$ [30]. On cooling down to $T = J/320$, short-range correlations apparently develops around the superlattice point $\mathbf{q}_{\rm sl} = \frac{2\pi}{a}(\frac{2}{3}, -\frac{2}{3}, 0)$ and symmetry-related points on the (111) plane (Fig. 4**b**). This correlation around $\mathbf{q}_{\rm sl}$ is found to be anisotropic. Along the cut $\frac{2\pi}{a}(h, -h, 0)$ within the (111) plane, the peak sharpens on cooling (Fig. 4**c**), while along an out-of-plane direction $\frac{2\pi}{a}(l + \frac{2}{3}, l - \frac{2}{3}, l)$, the intensity remains to be flat within errorbars (Fig. 4**d**). Besides, the peak intensity at $\mathbf{q}_{\rm sl}$ starts increasing rapidly on cooling below $T \sim 0.01J$ (Fig. 4**e**). It is likely that the ground state has a two-dimensional long-range order enlarging the unit cell by $\sqrt{3} \times \sqrt{3}$ as in the single-layer quantum kagomé spin ice model [13] (Fig. 2**i**). At present, however, it is difficult to reliably collect lower temperature data on our pyrochlore model with quantum Monte-Carlo simulations.

So far, there has been no concrete experimental evidence of the U(1) quantum spin liquid in candidate quantum spin ice materials at zero magnetic field. In a particular case of praseodymium pyrochlores, a step in the magnetization curve has already been observed in $Pr_2Ir_2O_7$ [27] most likely as a precursor to the 2/3 magnetization plateau. A careful annealing under a [111] magnetic field might lead to the quantum kagomé valence bond solid. Then, it will also be possible to observe the monopole supersolid by increasing the field above the plateau and measuring both the magnetization and the electric quadrupole moments with polarized neutron scattering experiments. The monopole supersolid phase, if observed, is a manifestation of a quantumness in spin ice and of monopoles.

Methods

Quantum Monte-Carlo calculations. All the numerical results presented here have been obtained by unbiased world-line QMC simulations based on the path integral formulation with continuous imaginary time. [31] To efficiently update the world-line configurations, we employed a worm algorithm with virtual placement of diagonal vertices.[25,32] Careful numerical annealing was employed on cooling to combat the severe freezing problems the quantum spin ice model is subject to. Statistical errors where computed by bootstrap analysis on a set of independent simulation series.

In particular, the results presented in Fig. 4 were obtained as follows: 16 independent parallel simulations were performed with the following series of cooling steps: $1/T = 0.01, 0.02, 0.04, \ldots, 0.32, 0.64, 1, 2, 3, \ldots, 99, 100, 102, 104, 106, \ldots$. At each temperature, 2×10^5 worm loops were generated for equilibration of the state inherited from the previous higher temperature. Then, measurements were performed during 3×10^6 loop updates.

Connection between the spin stiffness and the monopole superfluid stiffness. First, we summarize a mapping of the spin model H_{XXZ} onto a lattice Abelian Higgs model as given in refs [26,33].

We introduce an analogous "electric field" as a directed diamond-lattice link operator

$$E_{\mathbf{R}_+,\mathbf{R}_+ + 2\mathbf{b}_\mu} = -\mathrm{S}^z_{\mathbf{R}_+ + \mathbf{b}_\mu}. \tag{4}$$

Then, the monopole charge operator takes the form of an analogous "electric charge" satisfying the "Gauss law",

$$Q_{\mathbf{R}_\sigma} = \sum_\mu E_{\mathbf{R}_\sigma,\mathbf{R}_\sigma + 2\sigma\mathbf{b}_\mu}. \tag{5}$$

Monopolar spinon operators $\Phi_{\mathbf{R}} = e^{-i\varphi_{\mathbf{R}}}$ and $\Phi^\dagger_{\mathbf{R}} = e^{i\varphi_{\mathbf{R}}}$ are defined as annihilation-creation operators of $Q_{\mathbf{R}}$,

$$[\varphi_{\mathbf{R}}, Q_{\mathbf{R}'}] = i\delta_{\mathbf{R},\mathbf{R}'}, \quad [\Phi_{\mathbf{R}}, Q_{\mathbf{R}'}] = \Phi_{\mathbf{R}}\delta_{\mathbf{R},\mathbf{R}'}. \tag{6}$$

We further introduce the "vector potential" $A_{\mathbf{R},\mathbf{R}+\mathbf{b}_\mu}$ as another directed diamond-lattice link variable canonical connjugate to $E_{\mathbf{R},\mathbf{R}+\mathbf{b}_\mu}$,

$$[E_{\mathbf{R}_+,\mathbf{R}_+ + 2\mathbf{b}_\mu}, A_{\mathbf{R}'_+,\mathbf{R}'_+ + 2\mathbf{b}_\nu}] = i\delta_{\mathbf{R}_+,\mathbf{R}'_+}\delta_{\mu,\nu}. \tag{7}$$

Then, the transverse components of the spins can be written as

$$S^+_{\mathrm{R}_+ + \mathbf{b}_\mu} = \Phi^\dagger_{\mathbf{R}_+} e^{iA_{\mathbf{R}_+, \mathbf{R}_+ + 2\mathbf{b}_\mu}} \Phi_{\mathbf{R}_+ + 2\mathbf{b}_\mu}, \tag{8}$$

so that the commutation relation $[S^z_{\mathbf{r}}, S^+_{\mathbf{r}'}] = \delta_{\mathbf{r},\mathbf{r}'} S^+_{\mathbf{r}}$ is satisfied.

The spin stiffness parallel and perpendicular to the [111] field is given by

$$\rho_{[111]} = -\frac{1}{\beta L^3} \langle I^2_{[111]} \rangle, \quad \rho_{(111)} = -\frac{1}{2\beta L^3} \langle I^2_{(111)} \rangle \tag{9}$$

with

$$I^z_{[111]} = \mathbf{e}^z_0 \cdot \mathbf{I}^z, \quad \mathbf{I}^z_{(111)} = \mathbf{I}^z - I^z_{[111]} \mathbf{e}^z_0, \tag{10}$$

where

$$\mathbf{I}^z = i \frac{J_\perp}{2} \sum_{\langle \mathbf{r}, \mathbf{r}' \rangle} (\mathbf{r} - \mathbf{r}') \left(S^+_{\mathbf{r}} S^-_{\mathbf{r}'} - S^-_{\mathbf{r}} S^+_{\mathbf{r}'} \right) \tag{11}$$

represents the total spin current associated with S^z. This is exactly half the total monopole current $\mathbf{I}^m$;

$$\mathbf{I}^z = \frac{1}{2} \mathbf{I}^m, \quad \mathbf{I}^m = i \frac{J_\perp}{2} \sum_{\sigma = \pm} \sigma \sum_{\mathbf{R}_\sigma} \sum_{\mu \neq \nu} 2(\mathbf{b}_\mu - \mathbf{b}_\nu) \Phi^\dagger_{\mathbf{R}_\sigma + 2\sigma \mathbf{b}_\mu} e^{-i(A_{\mathbf{R}_\sigma, \mathbf{R}_\sigma + 2\sigma \mathbf{b}_\mu} - A_{\mathbf{R}_\sigma, \mathbf{R}_\sigma + 2\sigma \mathbf{b}_\nu})} \Phi_{\mathbf{R}_\sigma + 2\sigma \mathbf{b}_\nu} \tag{12}$$

and therefore, the spin stiffness is nothing but the superfluid stiffness of monopoles.

Note that the current spin model is also equivalent to the hard-core boson model having not only the nearest-neighbor hopping and repulsive interaction [24] but also an ionic potential without a chemical potential shift.

1. Molavian, H. R., Gingras, M. J. P. & Canals, B. Dynamically induced frustration as a route to a quantum spin ice state in $tb_2ti_2o_7$ via virtual crystal field excitations and quantum many-body effects. *Phys. Rev. Lett.* **98**, 157204 (2007).

2. Onoda, S. & Tanaka, Y. Quantum melting of spin ice: emergent cooperative quadrupole and chirality. *Phys. Rev. Lett.* **105**, 047201 (2010).

3. Hermele, M., Fisher, M. P. A. & Balents, L. Pyrochlore photons: The $U(1)$ spin liquid in a $S = \frac{1}{2}$ three-dimensional frustrated magnet. *Phys. Rev. B* **69**, 064404 (2004).

4. Moessner, R. & Ramirez, A. Geometrical frustration. *Phys. Today* **59**, 24 (2006).

5. Cornelius, A. L. & Gardner, J. S. Short-range magnetic interactions in the spin-ice compound $Ho_2Ti_2O_7$. *Phys. Rev. B* **64**, 060406(R) (2001).

6. Fukazawa, H., Melko, R. G., Higashinaka, R., Maeno, T. & Gingras, M. J. P. Magnetic anisotropy of the spin-ice compound $Dy_2Ti_2O_7$. *Phys. Rev. B* **65**, 054410 (2002).

7. Sakakibara, T., Tayama, T., Hiroi, Z., Matsuhira, K. & Takagi, S. Observation of a liquid-gas-type transition in the pyrochlore spin ice compound $Dy_2Ti_2O_7$ in a magnetic field. *Phys. Rev. Lett.* **90**, 207205 (2003).

8. Castelnovo, C., Moessner, R. & Sondhi, S. L. Magnetic monopoles in spin ice. *Nature* **451**, 42–45 (2008).

9. Brooks-Bartlett, M. E., Banks, S. T., Jaubert, L. D. C., Harman-Clarke, A. & Holdsworth, P. C. W. Magnetic-moment fragmentation and monopole crystalization. *Phys. Rev. X* **4**, 011007 (2014).

10. Andreev, A. F. & Lifshitz, L. M. Quantum theory of defects in crystals. *Sov. Phys. JETP* **29**, 1107–1113 (1969).

11. Chester, G. V. Speculations on Bose-Einstein condensation and quantum crystals. *Phys. Rev. A* **2**, 256–258 (1970).

12. Leggett, A. J. Can a solid be "superfluid"? *Phys. Rev. Lett.* **25**, 1543–1546 (1970).

13. Isakov, S. V., Wessel, S., Melko, R. G., Sengupta, K. & Kim, Y. B. Hard-core bosons on the kagome lattice: Valence-bond solids and their quantum melting. *Phys. Rev. Lett.* **97**, 147202 (2006).

14. Gardner, J. S., Gingras, M. J. P. & Greedan, J. E. Magnetic pyrochlore oxides. *Reviews of Modern Physics* **82**, 53 (2010).

15. Harris, M. J., Bramwell, S. T., McMorrow, D. F., Zeiske, T. & Godfrey, K. W. Geometrical frustration in the ferromagnetic pyrochlore $Ho_2Ti_2O_7$. *Phys. Rev. Lett.* **79**, 2554–2557 (1997).

16. Bramwell, S. T. & Gingras, M. J. P. Spin ice state in frustrated magnetic pyrochlore materials. *Science* **294**, 1495–1501 (2001).

17. Onoda, S. Effective quantum pseudospin-1/2 model for Yb pyrochlore oxides. *J. Phys.: Conf. Series* **320**, 012065 (2011).

18. Chang, L.-J. *et al.* Higgs transition from a magnetic coulomb liquid to a ferromagnet in $Yb_2Ti_2O_7$. *Nature communications* **3**, 992 (2012).

19. Bernal, J. & Fowler, R. A theory of water and ionic solution, with particular reference to hydrogen and hydroxyl ions. *J. Chem. Phys.* **1**, 515–548 (1933).

20. Ross, K. A., Savary, L., Gaulin, B. D. & Balents, L. Quantum excitations in quantum spin ice. *Phys. Rev. X* **1**, 021002 (2011).

21. Takatsu, H. *et al.* Quadrupole order in the frustrated pyrochlore $Tb_{2+x}Ti_{2-x}O_{7+\delta}$. *Phys. Rev. Lett.* **116**, 217201 (2016).

22. Kimura, K. *et al.* Quantum fluctuations in spin-ice-like $Pr_2Zr_2O_7$. *Nature communications* **4**, 1934 (2013).

23. Onoda, S. & Tanaka, Y. Quantum fluctuations in the effective pseudospin-1/2 model for magnetic pyrochlore oxides. *Phys. Rev. B* **83**, 094411 (2011).

24. Banerjee, A., Isakov, S. V., Damle, K. & Kim, Y. B. Unusual liquid state of hard-core bosons on the pyrochlore lattice. *Phys. Rev. Lett.* **100**, 047208 (2008).

25. Kato, Y. & Onoda, S. Numerical evidence of quantum melting of spin ice: qunatum-to-classical crossover. *Phys. Rev. Lett.* **115**, 077202 (2015).

26. Lee, S. B., Onoda, S. & Balents, L. Generic quantum spin ice. *Phys. Rev. B* **86**, 104412 (2012).

27. Machida, Y., Nakatsuji, S., Onoda, S., Tayama, T. & Sakakibara, T. Time-reversal symmetry breaking and spontaneous Hall effect without magnetic dipole order. *Nature* **463**, 210–213 (2010).

28. Sibille, R. *et al.* Candidate quantum spin ice in the pyrochlore $Pr_2Hf_2O_7$. *Phys. Rev. B* **94**, 024436 (2016).

29. Mirebeau, I., Bonville, P. & Hennion, M. Magnetic excitations in $Tb_2Sn_2O_7$ and $Tb_2Ti_2O_7$ as measured by inelastic neutron scattering. *Phys. Rev. B* **76**, 184436 (2007).

30. Tabata, Y. *et al.* Kagomé ice state in the dipolar spin ice $Dy_2Ti_2O_7$. *Phys. Rev. Lett.* **97**, 257205 (2006).

31. Kawashima, N. & Harada, K. Recent Developments of World-Line Monte Carlo Methods. *J. Phys. Soc. Jpn.* **73**, 1379 (2004).

32. Kato, Y., Suzuki, T. & Kawashima, N. Modification of directed-loop algorithm for continuous space simulation of bosonic systems. *Phys. Rev. E* **75**, 066703 (2007).

33. Savary, L. & Balents, L. Coulomb quantum liquids in spin-1/2 pyrochlores. *Phys. Rev. Lett.* **108**, 037202 (2012).

Acknowledgements The work was partially supported by Grants-in-Aid for Scientific Research under Grant No. 24740253 and No. 15H03692 from Japan Society for the promotion of Science and under Grant No. 15H01025 from the Ministry of Education, Culture, Sports, and Technology of Japan and by the RIKEN iTHES project. Numerical computationss were performed by using the HOKUSAI-Great Wave supercomputing system at RIKEN.

Author Contributions The authors equally contributed to the work.

Competing Interests The authors declare no competing financial interests.

Correspondence Correspondence and requests for materials should be addressed to S.O. (s.onoda@riken.jp).

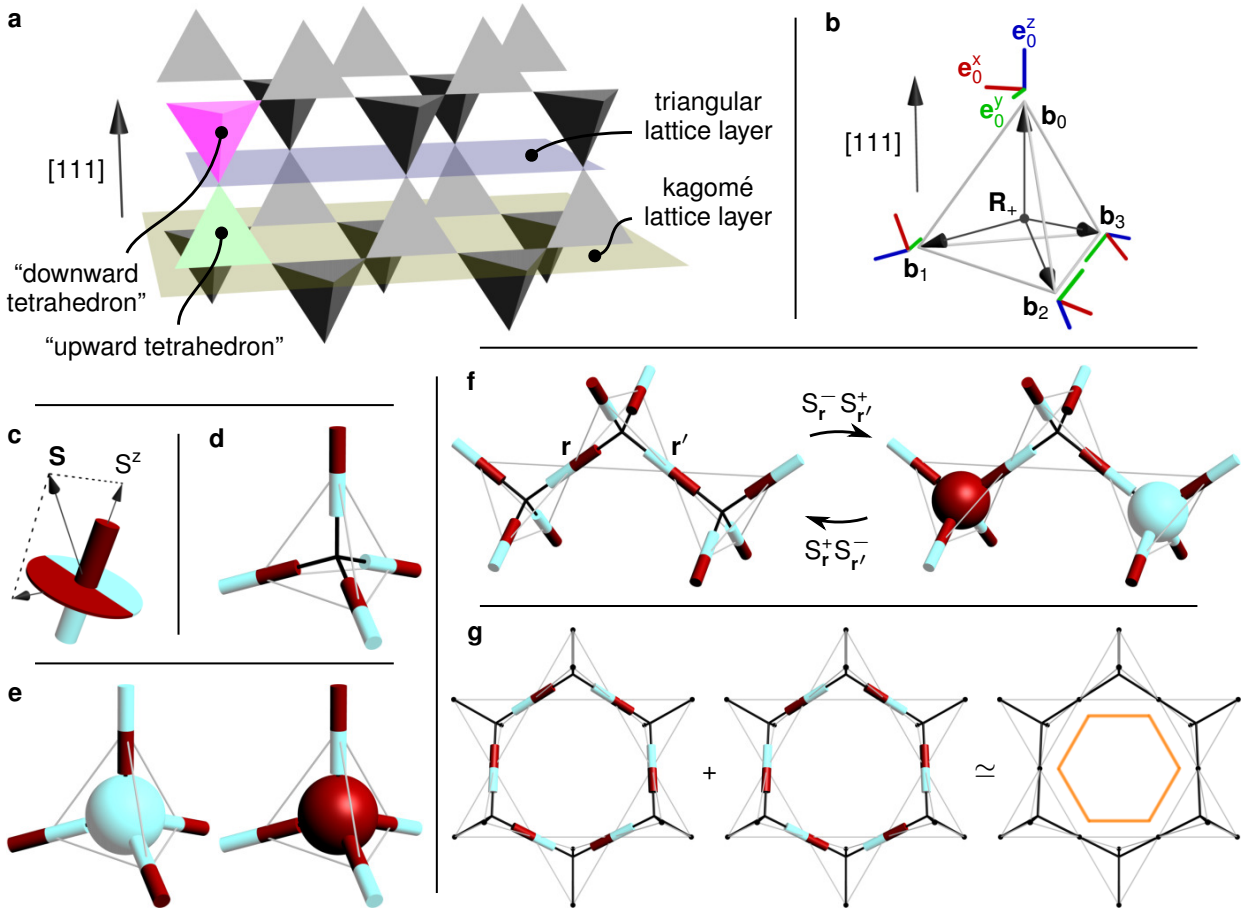

Figure 1: **Building blocks of quantum spin ice. a** and **b**, The pyrochlore lattice structure. A pyrochlore lattice site is expressed as $\mathbf{r} = \mathbf{R}_\pm \pm \mathbf{b}_\mu$, with a center of an upward/downward tetrahedron $\mathbf{R}_\pm$ and four sublattice vectors $\mathbf{b}_\mu$ ($\mu = 0, \cdots, 3$). A global [111] direction and (111) kagomé and triangular lattice layers are also shown. **c**, A pictorial representation of a spin, **S**, decomposed into a – with respect to a local z-axis $\mathbf{e}^z_\mu$ – parallel component (rod) and perpendicular component (disk). **d** and **e**, 2-in, 2-out and 3-in, 1-out (1-in, 3-out) configurations, respectively, of four spins situated at the coners of a tetrahedron. The latter contains a +1/-1 monopole charge, depicted by the colored balls at the centers of the tetrahedra. The color and size of the balls illustrates the sign and magnitude of the charge, respectively. **f**, A spin exchange process leads to the creation/annihilation – and successive exchanges to propagation – of monopole pairs. Note that $\mathbf{S}^\pm_\mathbf{r} \equiv \mathbf{S}^x_\mathbf{r} \pm i\mathbf{S}^y_\mathbf{r}$. **g**, In quantum spin ice, states may tunnel into each other without invoking the energy cost of creating monopole pairs. Here the lowest order process, a hexagon ring exchange, is depicted as the superposition of clockwise and anti-clockwise spin arrangements around a pyrochlore lattice hexagon. Longer exchange paths can be constructed from superimposing adjacent hexagon paths.

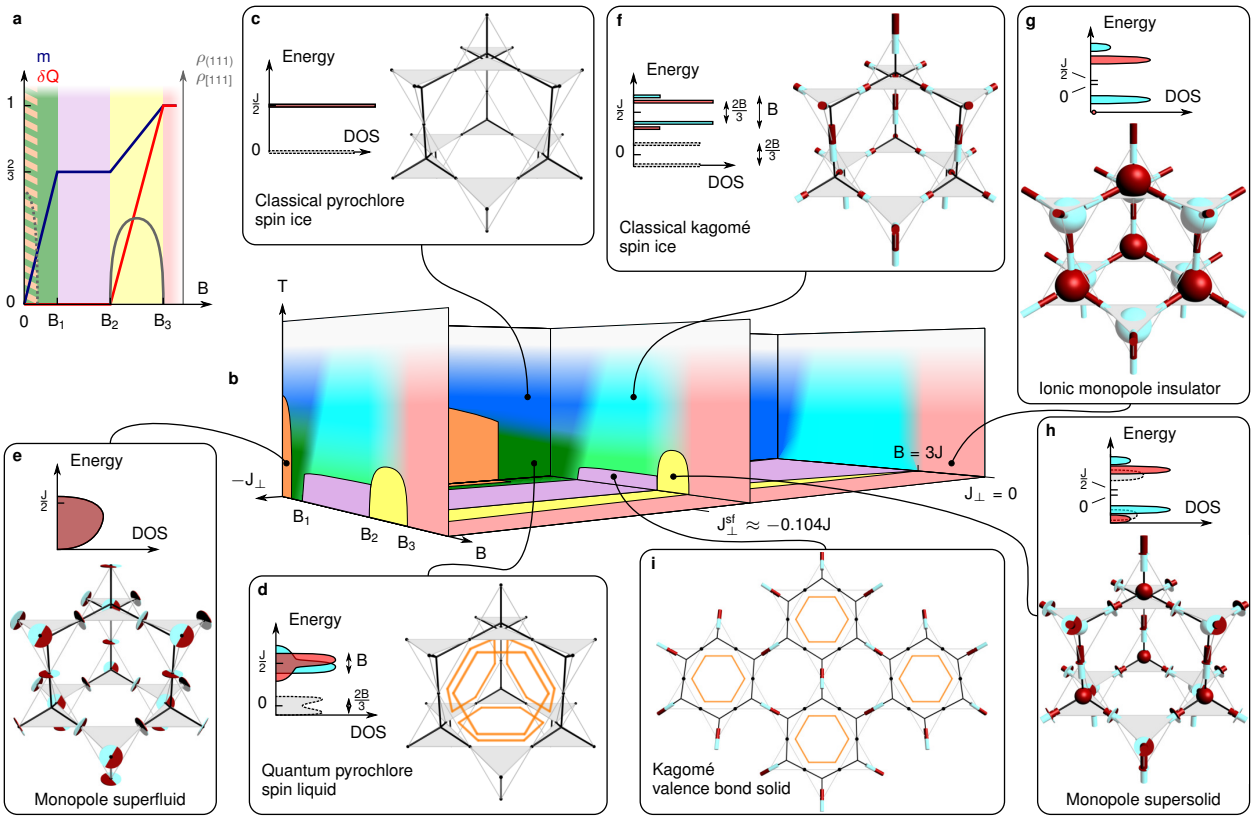

Figure 2: **Global phase diagram of the minimal pyrochlore quantum spin ice model.** **a**, Schematic illustration of m, δQ, $\rho_{(111)}$ and $\rho_{[111]}$ as functions of B in the ground state. **b**, The global $J_\perp$-B-T phase diagram obtained by QMC simulations. **c**–**h**, Illustrations of the excitation spectrum, as well as the average spatial profiles of spins and monopoles in the classical spin ice regime (**c**), U(1) quantum spin liquid regime (**d**), monopole superfluid phase (**e**), classical kagomé spin ice regime (**f**), ionic monopole insulator with a full 3-in, 1-out spin polarization (**g**), and monopole supersolid (**h**). For excitation spectra, the monopole charge sectors are colored based on whether $Q = -1$ (cyan), $Q = 0$ (gray), or $Q = +1$ (red). For graphical representations of spins and monopoles, see Fig. 1). **i**, Average spin and monopole profile on a single kagomé plane in the kagomé valence bond solid phase. In **a** and **b**, transitions and crossovers between phases and regimes are illustrated by sharp lines and gradients between different colors, respectively. In **a**, Depending on the magnitude of $J_\perp$, the spin stiffnesses $\rho_{(111)}$, $\rho_{[111]}$ in the vicinity of zero field $B \sim 0$ may either be zero, as is the case for the quantum pyrochlore spin liquid regime (**d**), or finite, as for the monopole superfluid phase (**e**). At B_1 the system enters the 2/3 kagomé spin ice magnetization plateau (**i**). In the classical limit $J_\perp = 0$, B_1 decays to zero, while it is finite for $J_\perp \neq 0$. At B_2 the 2-in, 2-out spin ice rule breaks down and the ionized monopole charge δQ becomes finite. A supersolid phase (**h**) emerges and lasts until the spin polarization saturates at B_3. For $B > B_3$ we have a monopole ionic insulator (**g**) with a perfect ionization of monopoles.

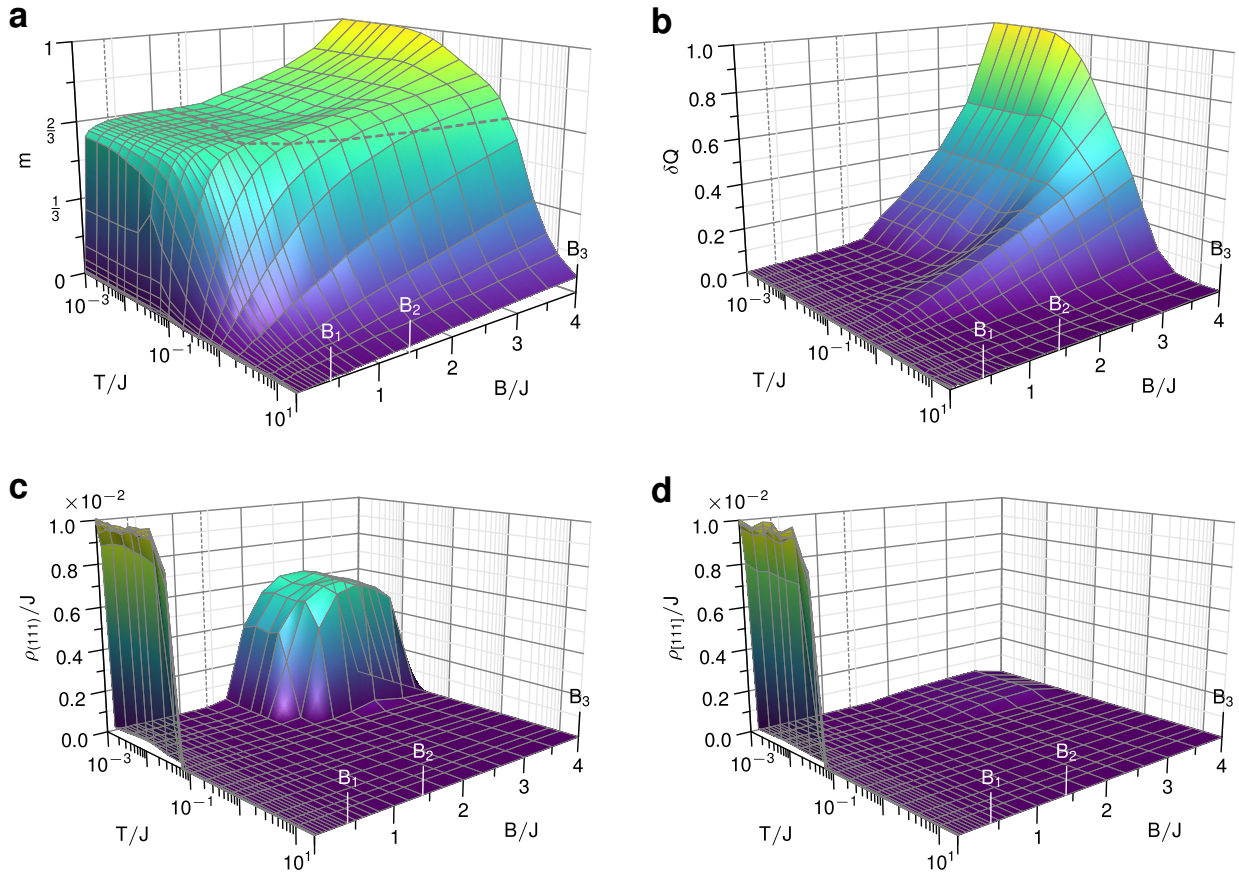

Figure 3: **Quantum Monte-Carlo results on thermodynamic properties. a**, The [111] magnetization per spin. **b**, The ionized monopole charge per tetrahedron. **c** and **d**, The transverse spin stiffness normal and parallel to the [111] magnetic field. For all plots, $J_\perp = -0.15J$ and $L = 10$. Each mesh vertex represents one QMC data point. Statistical errorbars are invisibly small, except in the low-temperature region of the monopole superfluid phase in **c** and **d**, where they are at most 3×10^{-4}.

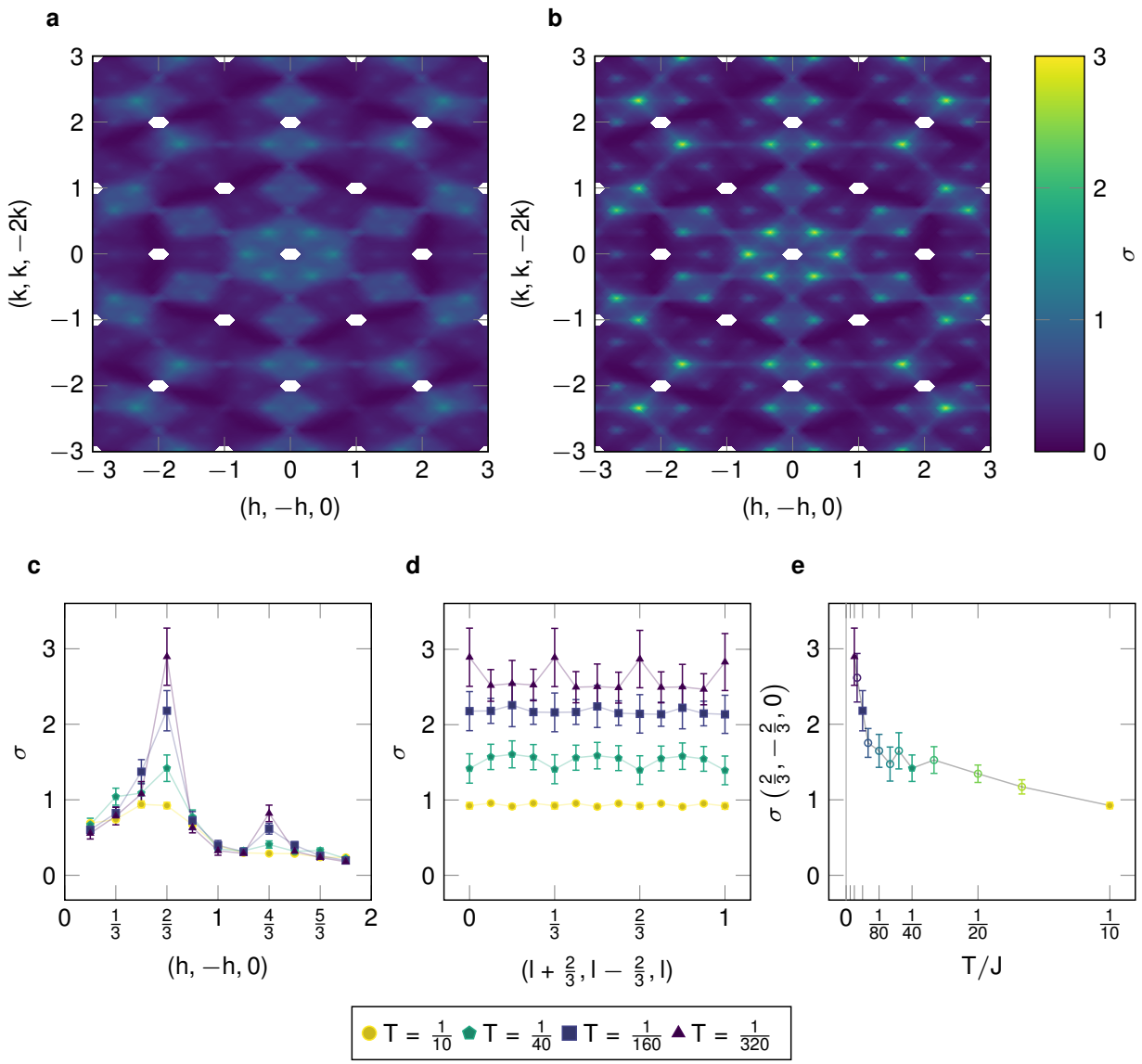

Figure 4: **Spatial profiles of diffuse neutron-scattering cross-sections. a–e**, Equal-time (energy-integrated) neutron-scattering cross-sections $\sigma(\mathbf{q}) = \sum_{\mu,\nu=0}^{3}\langle S^z_{\mu,\mathbf{q}} S^z_{\nu,-\mathbf{q}}\rangle \left(\mathbf{e}^z_\mu \cdot \mathbf{e}^z_\nu - \frac{(\mathbf{q}\cdot\mathbf{e}^z_\mu)(\mathbf{q}\cdot\mathbf{e}^z_\nu)}{q^2}\right)$ with $S^z_{\mu,\mathbf{q}} = \frac{1}{L^{3/2}}\sum_{\mathbf{R}} e^{-i\mathbf{q}\cdot(\mathbf{R}+\mathbf{b}_\mu)}$ are shown in the reciprocal lattice plane $\mathbf{q} = (2\pi/a)(h+k, -h+k, -2k)$ perpendicular to the magnetic field. **a**, The classical kagome spin ice regime, $(J_\perp, B, T) = (-0.15, 1.3, 1/20)J$. **b**, A short-range ordered state towards the kagome valence bond solid [13], $(J_\perp, B, T) = (-0.15, 1.3, 1/320)J$. The Bragg peaks due to the polarized triangular lattice spins have been subtracted in both **a** and **b**. **c** and **d**, $\sigma(\mathbf{q})$ for q along the $(h, -h, 0)$ line (perpendicular to the field) and along the $(l + \frac{2}{3}, l - \frac{2}{3}, l)$ line (parallel to the field) for various temperatures. The lines are chosen to go through the position of the superlattice Bragg peak observed in the associated 2D quantum kagomé spin ice model at zero temperature [13]. **e**, Temperature dependence of the peak intensity at $\mathbf{q} = (2\pi/a)(\frac{2}{3}, -\frac{2}{3}, 0)$. $L = 12$ for all the panels.